TITLE: Endosomal sorting protein SNX4 limits synaptic vesicle docking and release

Authors: Poppinga, J [1]*, Barret, N.J. [1], Cornelisse, L.N. [1,2], Verhage, M.[1,2], van Weering, J.R.T. [1,2#]
[1]Department of Functional Genomics, Center for Neurogenomics and Cognitive Research (CNCR), VU University, Amsterdam, The Netherlands and [2]Department of Human Genetics, CNCR, Amsterdam UMC, Amsterdam, the Netherlands
corresponding author: Jan R.T. van Weering, De Boelelaan 1085, 1081 HV, Amsterdam, The Netherlands, jan.van.weering@vu.nl, +31 (0) 20 5986930

Keywords: Endosome sorting, neurotransmission, SNX4, hippocampal neurons

Sorting nexin 4 (SNX4) is an evolutionary conserved organizer of membrane recycling. In neurons, SNX4 accumulates in synapses, but how SNX4 affects synapse function remains unknown. We generated a conditional SNX4 knock-out mouse model and report that SNX4 cKO synapses show enhanced neurotransmission during train stimulation, while the first evoked EPSC was normal. SNX4 depletion did not affect vesicle recycling, basic autophagic flux or the levels and localization of SNARE-protein VAMP2/synaptobrevin-2. However, SNX4 depletion affected synapse ultrastructure: an increase in docked synaptic vesicles at the active zone, while the overall vesicle number was normal, and a decreased active zone length. These effects together lead to a substantially increased density of docked vesicles per release site. In conclusion, SNX4 is a negative regulator of synaptic vesicle docking and release. These findings suggest a role for SNX4 in synaptic vesicle recruitment at the active zone.

Endosome sorting plays a critical role in the recycling and degradation of proteins in various eukaryotic cell types, including neurons (Cullen & Steinberg, 2018; Huotari & Helenius, 2011; Sardana & Emr, 2021; Vietri et al., 2020). Synapses, in particular, rely on rapid recycling mechanisms to replenish synaptic vesicles (SVs) and facilitate neurotransmitter release (Kononenko & Haucke, 2015; Rizzoli, 2014; Südhof, 2000). The extent to which endosome sorting is involved in these processes has been a subject of ongoing debate since the early studies on SV recycling (Ceccarelli et al., 1973; Heuser & Reese, 1973; Kononenko & Haucke, 2015; Watanabe & Boucrot, 2017). While it has been demonstrated that depleting endosomal proteins affect neurotransmitter release (Chen et al., 2017; Tagliatti et al., 2016; Uytterhoeven et al., 2011), the precise role of these sorting proteins on SV maintenance and fusogenity remains not well understood.

Sorting nexins (SNXs) are evolutionary conserved organizers of endosome sorting that are recruited to endosome membrane domains by a phox homology (PX) domain (Carlton et al., 2005). SNX4 belongs to a subgroup of SNXs containing a C-terminal a Bin–Amphiphysin–Rvs (BAR) domain that recognizes and remodels curved endosome membranes (Cullen & Steinberg, 2018; Teasdale et al., 2001; Van Weering et al., 2012). While several SNX-BARs are associated with the retromer-related Endosomal SNX-BAR Sorting Complex for Promoting Exit (ESCPE)-1 (Simonetti et al., 2023), SNX4 forms a distinct sorting complex with SNX7, SNX30 (Antón et al., 2020; van Weering et al., 2012), SNX5 (Zhou et al., 2022), or SNX32 (Sugatha et al., 2023) for endosome-to-cell surface recycling pathways and autophagosome traffic (Traer et al., 2007; Van Weering et al., 2012; Zhou et al., 2022). SNX4 emerges as a central hub in this endosome recycling pathway as the expression of SNX4 is required for the stable SNX7 and SNX30 protein levels in cells (Antón et al., 2020). SNX4 is expressed in all cell types but to what extent this conserved principle also operates in highly polarized mammalian cells, such as neurons, remains unclear. In post-mortem brain material of

Alzheimer's disease patients, altered protein levels of SNX4 have been observed (Kim et al., 2017). SNX4 is implicated in the recycling of the amyloid precursor protein cleaving enzyme (BACE-1), sorting it away from the endolysosomal pathway (Kim et al., 2017; Toh et al., 2018). Consequently, dysregulation of SNX4 may lead to the mislocalization of BACE-1 to late endosomal compartments, potentially contributing to altered amyloid-ß-production. In yeast, Snx4 is essential for the endosome recycling of Snc1p, a homolog of the SNARE protein VAMP2/synaptobrevin-2 (VAMP2/syb2) that is essential for synaptic transmission (Hettema et al., 2003; Ma et al., 2017; Schoch et al., 2001). In neurons, SNX4 specifically accumulates in synapses, and its knockdown dysregulates protein pathways involved in neurotransmission (Vazquez-Sanchez et al., 2020). While its synaptic subcellular localization has been shown, the functional role of SNX4-dependent endosome sorting in synapses remains unknown.

In this study, we characterize the role of endosomal sorting protein SNX4 in synapse function using a novel conditional SNX4 knock-out mouse model. We show that SNX4 limits synaptic vesicle docking and release. SNX4 depletion enhances neurotransmission specifically during train stimulation, while the first evoked response is not significantly affected. SNX4 depletion does not impact vesicle recycling or the levels and localization of the SNARE-protein VAMP2/syb-2. The overall number synaptic vesicles is unaffected in SNX4 cKO neurons, but these synapses show an increased number of docked synaptic vesicles at the active zone of the presynapse. The active zone length is decreased, thereby further increasing the density of synaptic vesicles at the release site of SNX4 cKO synapses. Our data collectively shows that the endosomal sorting protein SNX4 is a negative regulator of synaptic vesicle docking and release.

RESULTS

Neuronal SNX4 protein levels are depleted in 21 days in conditional SNX4 knock out mouse primary cultures.

We generated a conditional knock-out mouse model for SNX4 (Fig. 1a and materials and methods section) to circumvent previously reported off-target effects using shRNA approaches (Vazquez-Sanchez et al., 2020). In neuronal cultures, SNX4 has a half lifetime of 10.6 days (Dörrbaum et al., 2018). To test SNX4 optimal knock out efficiency, cKO neurons were fixed after 21 days *in vitro* (DIV21) and Cre expression was initiated at different time points (DIV7, DIV3, and DIV0) (Fig. 1b). SNX4 expression was detected by western blot which showed a reduction of 67% after 14 days of cre, 83% after 18 days of cre and 90% after 21 days of cre compared to control neurons infected with delta-Cre (Fig. 1c, d). Immunohistochemistry of SNX4 in primary hippocampal neurons showed a 64% reduction in SNX4 in MAP2-neurites after 21 days of expressing cre (Fig. 1e, f). Morphological parameters such as dendrite length and dendrite branching, based on MAP2 staining, and synapse number, based on VAMP2 puncta, remained unaffected in SNX4 cKO neurons (Fig. 1 f-i & Fig. 4a). These data show a successful depletion of 90% of endosomal sorting protein SNX4 using a novel conditional knock-out mouse model for SNX4.

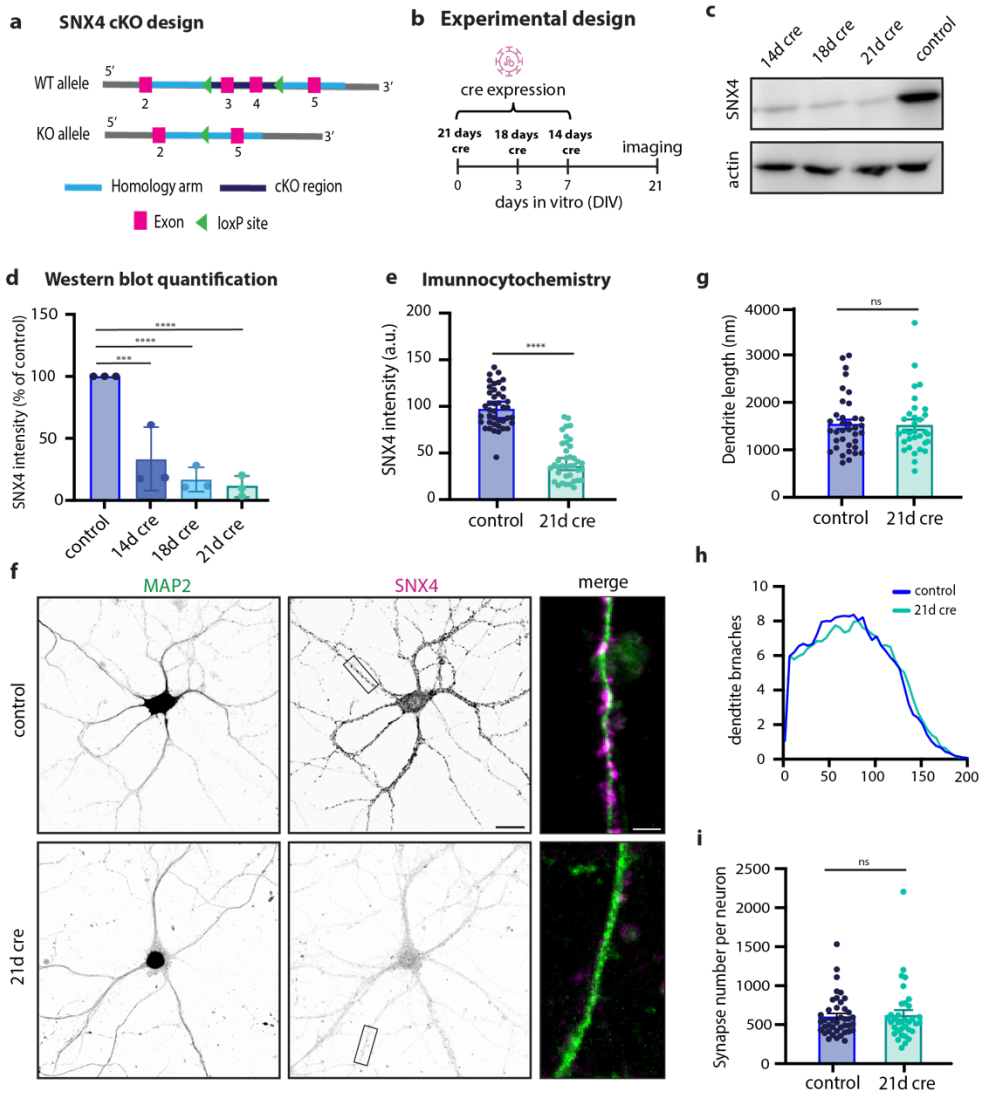

Figure 1: SNX4 is knocked-out in primary hippocampal neurons using a novel conditional knock-out mouse line. (a) Schematic overview of conditional knock-out design of SNX4. **(b)** Schematic overview of experimental design using cre intervention at different DIVs. **(c)** Typical example of western blot of SNX4 and actin at 14 days, 18 days and 21 days of cre and control (delta cre) expression. **(d)** Quantification of western blot SNX4 protein levels for control (dcre), 14 days of cre, 18 days of cre and 21 days of cre, normalized to control. **(e)** Quantification of immunocytochemistry SNX4 intensity normalized to control. **(f)** Typical example of primary hippocampal neurons stained for SNX4 (magenta) and map2 (green) for control and 21 days of cre. Scale bar = 20 µm. Zoom-in scale bar = 3 µm. **(g)** Dendrite length for control and KO hippocampal neurons. **(h)** Sholl analysis for number dendrite branches. **(i)** Number of synapses per neuron (MAP2 mask) based on VAMP2 puncta (shown in Fig. 4) ****p=<0.0001, ***p=0.0003, **p=0.0005, *p=0.0019. Ordinary one-way ANOVA with Tukey's multiple comparisons test for **(d)** with N=3 animals. Mann-Whitney test for **(e)** with n=32-42 neurons per group and N=6 animals and. Data points represent individual western blots/neurons; bar graph represents mean with SEM.

SNX4 depletion enhances neurotransmission during train stimulation

To investigate the functional role of SNX4 in synapses, we studied the effect of SNX4 depletion on neurotransmission by electrophysiological recordings in single hippocampal neurons cultured on glia micro-islands (autapse) at DIV21 (Fig. 2a). Both the amplitude and charge of the first evoked response showed a non-significant trend towards an increase in SNX4 cKO neurons (KO) compared to neurons infected with delta-Cre (control) (Fig. 2b, c & d). The rescue condition where SNX4 was re-expressed at DIV14 (KO + SNX4) showed a decreased amplitude compared to KO but not to control. A similar trend was observed for total charge (Fig. 2b, d). Paired pulse ratios were not affected in SNX4 cKO neurons (Fig. 2e). We next investigated the effect of SNX4 depletion on synaptic transmission during sustained activity using a series of train stimulations at 5, 10 and 40Hz (results in Supplementary table 1, Supplementary Fig S2). During a train of 100 action potentials at 40 Hz, the charge in SNX4 cKO neurons was highly increased (Fig. 2f, h). The average charge between pulse 90-100 was increased by 110% in SNX4 cKO synapses compared to control (Fig. 2g). SNX4 overexpression rescued this increase in charge to WT levels (Fig. 2f, g &h). The size and

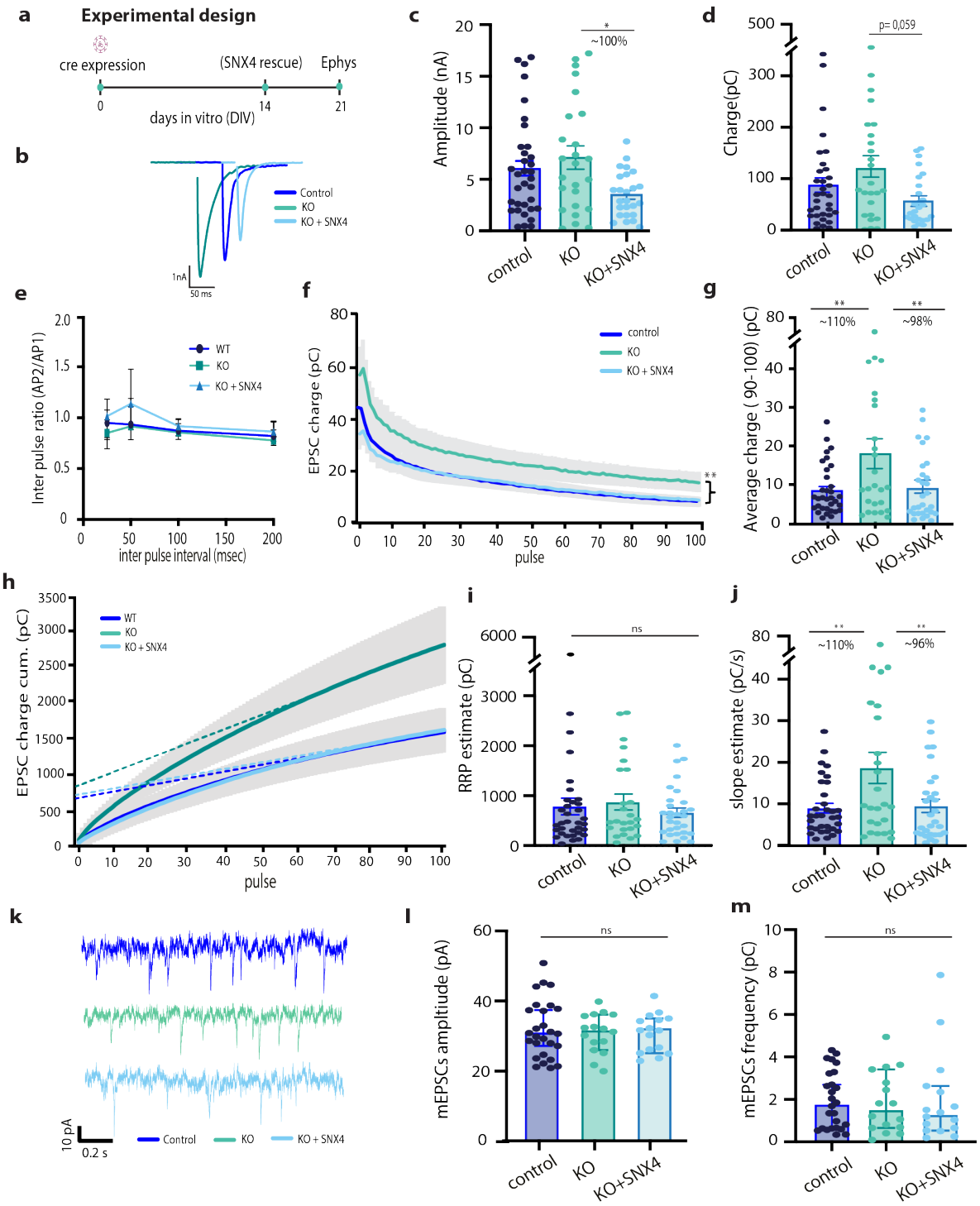

Figure 2: SNX4 depletion increases sustained synaptic vesicle release. (a) Schematic overview of experimental design using cre intervention at DIV0, SNX4 rescue at DIV14 and recording at DIV21. **(b)** Representative traces of the first evoked response for control, KO and KO+SNX4 upon stimulation. **(c)** Amplitude of first evoked response. **(d)** Charge of first evoked response. **(e)** Paired pulse ratios of amplitude at inter pulse intervals of 25, 50, 100 and 200 msec. **(f)** Mean EPSC charge trace for 100 AP at 40 Hz train. **(g)** Average charge at pulse 90-100. **(h)** Cumulative EPSC charge for 100 AP at 40 Hz train with back extrapolation linear fit to AP 80-100. **(i)** Estimate of RRP based on back extrapolation (h). **(j)** Estimate of slope based on based on back extrapolation **(k)** representative traces of mEPSC response for control, KO and KO+SNX4 **(l)** mEPSC amplitude (**m)** mEPSC frequency. Multilevel ANOVA with n = 25-38 neurons per group of N = 3-4 animals. ***p < 0.0001, **p < 0.001. Data points represent individual neurons; bar graph represents mean with SEM.

refilling of the readily releasable vesicle pool (RRP) was estimated using back extrapolation of the cumulative charge (Fig. 2h) (Schneggenburger et al., 1999). While we found no significant differences in RRP estimate size in SNX4 cKO synapses compared to control (Fig. 2i), the slope estimate of the cumulative charge was increased upon SNX4 depletion, which was rescued by SNX4 overexpression (Fig. 2j). The amplitude and frequency of spontaneous miniature EPSCs (mEPSCs) were not affected upon SNX4 depletion (Fig. 2k-m). In order to investigate a direct effect of SNX4 overexpression on neurotransmission, we expressed exogenous SNX4 on wild-type control background. Both the amplitude and charge of the first evoked response showed no effect in control + SNX4 neurons compared to control, and no differences were detected in the response to the 40 Hz stimulation train (Supplementary Fig. 3a-e), indicating that SNX4 overexpression in itself does not affect the neurotransmission protocols studied in SNX4 cKO experiments. Together these data show enhanced neurotransmission during train stimulation in SNX4 cKO autapses, while single EPSCs, mEPSCs and the RRP size estimate remain unaffected. This suggests that vesicle recruitment during high frequency train stimulation is limited by SNX4.

Synaptic vesicle recycling and retrieval are not altered in SNX4 cKO neurons.

As the recruitment rate of releasable vesicles during train stimulation was increased in SNX4 cKO neurons, we assessed its role in synaptic vesicle recycling using the synaptic vesicle fusion reporter synaptophysin-super-ecliptic-pHluorin (SypHy) (Granseth et al., 2006). Neurons were stimulated by two trains of 100 action potentials at 40 Hz. The total pool of SypHy in acidified SVs per synapse was determined by NH4 superfusion (Fig. 3a, b). SNX4 cKO neurons showed a higher fluorescence intensity upon both stimulation trains (Fig. 3c), represented as the stimulated fraction (Fig. 3d, e), and return to baseline fluorescence level within 60 seconds over a total imaging time course of 160 seconds (Fig. 3c). The fluorescence decay time constant tau in the 60 s after electrical stimulation, a measure for SV endocytosis, was not changed after both stimuli in SNX4 cKO neurons (Fig. 3f). Finally, the responding fluorescent puncta during action potential stimulation as a ratio of the total fluorescent puncta during NH4, the percentage of active synapses, showed a trend towards fewer active synapses in SNX4 cKO neurons (Fig. 3g). Hence, these data show that SNX4 depletion enhances synaptic vesicle release without altering synaptic vesicle recycling and the number of active synapses in hippocampal neurons.

It has, however, been shown that different SV recycling pathways dominate at different temperatures (Watanabe et al., 2013). To test if SNX4 affects SV recycling at physiological temperatures, we used a FM4-64 dye loading protocol before electrical field stimulation (Fig. 3h). Recycling SVs were labelled by a 60s-incubation with FM4-64 in 60mM K^+ at 37^0C. Vesicle fusion was triggered by a train of action potentials at 40 Hz, resulting in a decreased FM4-64 fluorescence intensity (Fig. 3h, i). SNX4 cKO neurons showed a similar fluorescence intensity decay after electrical stimulation over a total imaging time course of 80 seconds (Fig. 3j). The average fluorescence signal in the last 10 seconds normalized to baseline (F/F0), a measure for the total amount of recycling synaptic vesicles fusing, was not significantly different between control and SNX4 cKO neurons (Fig. 3k). FM4-64 uptake, a measure for endocytosis at 37 ^{0}C, was also not altered in SNX4 cKO neurons (Fig. 3l). Taken together, these data suggest that SNX4 depletion does not affect synaptic vesicle endocytosis and recycling both at room temperature and physiological temperature.

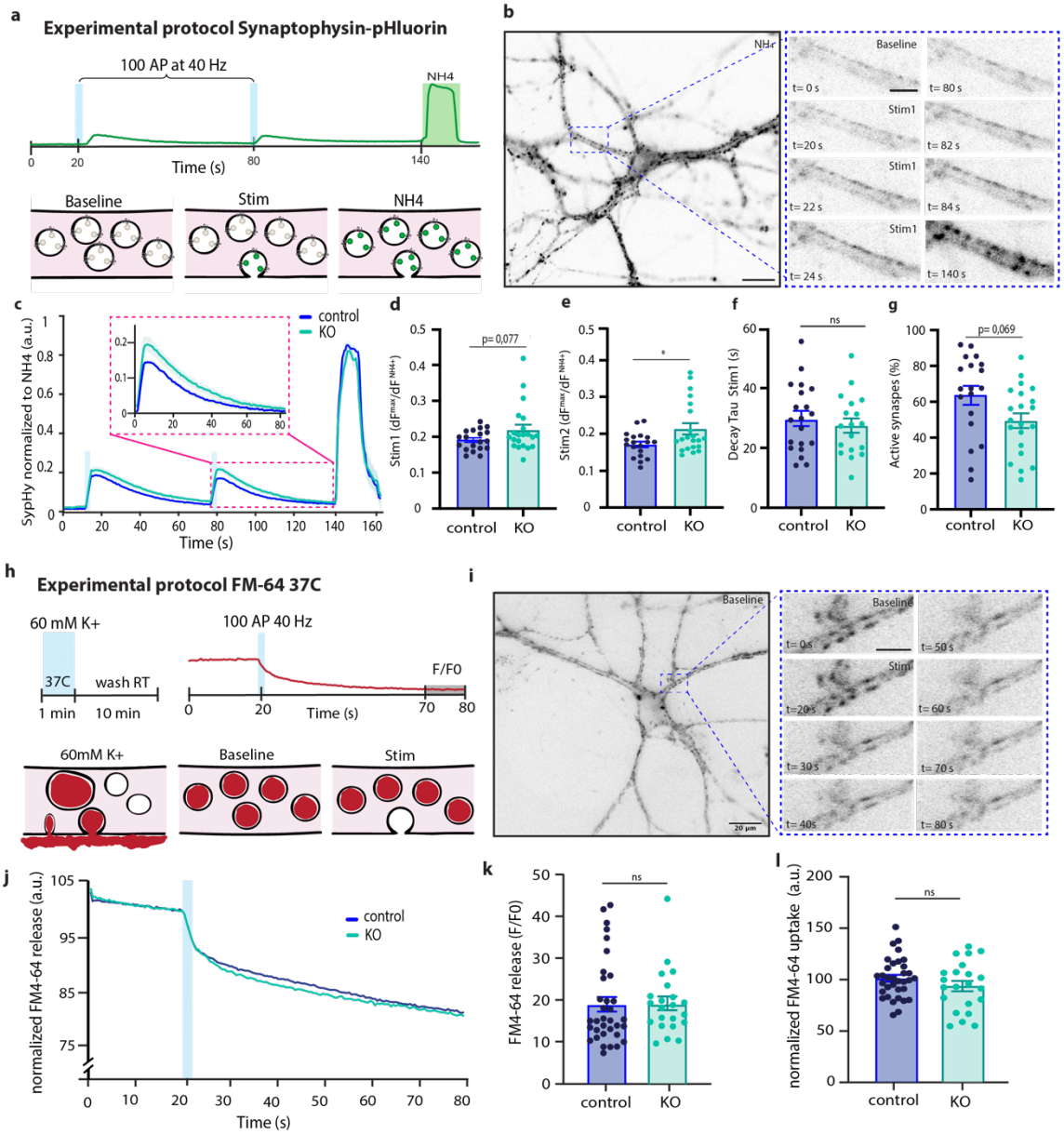

Figure 3: SNX4 depletion does not affect synaptic vesicle recycling at room temperature and physiological temperatures. **(a)** Stimulation paradigm with a single vesicle fluorescence intensity trace**. (b, Left)** Representative image of a SypHy–infected neuron during Tyrode's NH4 application (Scale bar: 20 µm.). **(Right)** Neurite before (baseline) and during (100 AP at 40 Hz) stimulation and during NH4 application (NH4) (Scale bar: 10 µm.). **(c)** The average fluorescence normalized from baseline to maximum SypHy intensity during Tyrode's NH4 application. **(d)** Maximum response amplitude during the first electrical stimulation normalized to maximum NH4 response plotted as $\Delta F^{max}/F^{NH4}$**. (e)** Maximum response amplitude during the second electrical stimulation normalized to maximum NH4 response plotted as $\Delta F^{max}/F^{NH4}$**. (f)** Fluorescence decay time constant tau in the 60 s after electrical stimulation representing SV endocytosis and acidification **(g)** Percentage active synapses. **(h)** Stimulation paradigm with a single vesicle fluorescence intensity trace**.** Recycling SVs are labelled by 60s-incubation with FM4-64 in 60mM K+ at 37C, followed by a 10min washout. Electrical field stimulation (100AP, 40Hz) triggers SV exocytosis recorded as decreased FM4-64 fluorescence intensity. **(i, Left)** Representative image of FM64-dye endocytosed by a neuron during baseline (Scale bar: 20 µm.). **(Right)** Neurite before (baseline) and during (100 AP at 40 Hz) stimulation (Scale bar: 10 µm.). **(j)** The average FM4-64 fluorescence traces, normalized to control baseline, over time showing initial SV loading, followed by release after electrical field stimulation. **(k)** FM4-64 release upon electrical field stimulation **(l)** FM4-64 uptake (upon 60 mm K^+ incubation). Multilevel ANOVA with N=3 animals and n=21-24 neurons per group for SypHy experiment and N=4 animals with n=28-36 neurons per group for FM64-dye experiment. Bar graph represents mean with SEM. Data points represent individual fields of view**.**

SNX4 depletion does not affect synaptic VAMP2/syb-2 levels and distribution or autophagy markers in neurons.

In yeast, it is reported that SNX4 homologue Snx4p mediates retrieval of Snc1p, yeast's VAMP2/syb-2 homologue (Hettema et al., 2003; Ma et al., 2017). Missorting of VAMP2 in neurons could affect synaptic transmission. Therefore, we investigated VAMP2/syb-2 as potential cargo of SNX4. To test whether SNX4 mediates VAMP2/syb-2 retrieval in neurons, we investigated the localization, number and expression levels of VAMP2/syb-2 upon SNX4 knock-out by immunohistochemistry. SNX4 immunostaining showed clear co-localization with VAMP2/syb-2 (Fig. 4a). In SNX4 cKO neurons, no significant difference was found in VAMP2/syb-2 puncta number per µm dendrite or VAMP2/syb-2 intensity (Fig. 4a, b, c). Sholl-analysis of average VAMP2/syb-2 intensity over distance from soma also revealed no differences in VAMP2/syb-2 localization upon SNX4 depletion (Fig. 4d). Western blot analysis revealed no changes in total VAMP2/syb-2 protein levels (Fig. 4e). These data show that SNX4 is not required for a normal VAMP2/syb-2 distribution and protein level, as observed for the yeast orthologs of both proteins. Other potential cargos of SNX4 that could affect neurotransmission include those involved in the autophagy pathway (Antón et al., 2020; Kuijpers et al., 2021). We investigated autophagy markers and autophagosomes following SNX4 depletion, using P62 as a basal autophagic receptor marker and bafilomycin to inhibit autolysosome formation, thereby assessing basal autophagic flux. In SNX4 cKO neurons, there was no significant difference in P62 puncta numbers or P62 somatic intensity under basal conditions or after bafilomycin treatment, suggesting that autophagic flux remains normal (Supplementary Fig. 4a, b, c). Western blot analysis also showed no changes in total ATG5 protein levels (Supplementary Fig. 4d&e) and ultrastructural analysis revealed no differences in the total number of autophagosomes (Supplementary Fig. 4f&g). Collectively, these data indicate that SNX4 depletion does not impact the basal autophagic flux, ATG5 protein levels, or the number of autophagosomes.

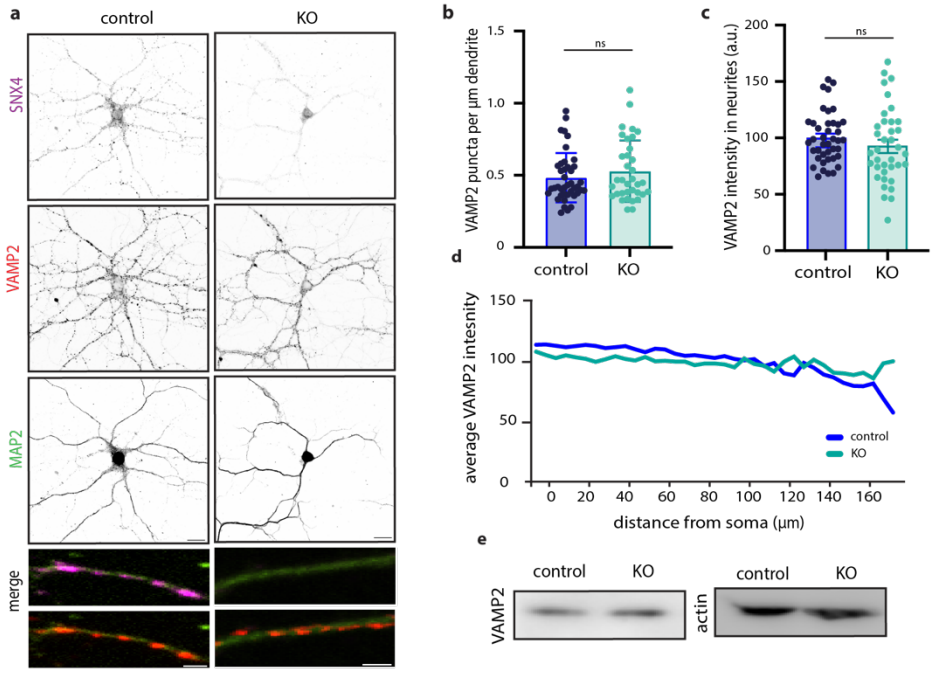

Figure 4: SNX4 depletion does not decrease VAMP2 levels and localization. (a) Typical example immunocytochemistry images of primary hippocampal neurons stained for SNX4 (magenta), VAMP2 (red) and MAP2 (green) from control and SNX4 cKO mice. Scale bar = 20 µm. Merge zoom-in scale bar = 2 µm. **(b)** VAMP2 puncta per µm dendrite for control and KO. **(c)** VAMP2 intensity measured in dendrites. **(d)** Sholl analysis of average VAMP2 intensity over distance from the soma for control and KO. **I** Western blot of SNX4, VAMP2, and actin for control and KO. Data points represent individual neurons, N=6 animals and n=35-41 neurons for VAMP2 data, bar graphs represent mean with SEM.

Presynaptic ultrastructure and synaptic vesicle docking are affected in SNX4 cKO synapses.

Next, we sought to further investigate synapse organization upon SNX4 depletion using electron microscopy (Fig 5a). The number of docked vesicles was measured by direct contact of vesicles with the active zone plasma membrane (Fig. 5a,b). The average synaptic vesicle size, defined by all clear core vesicles smaller than 50 nm, was reduced by 5%, whereas vesicles larger than 50 nm, did not show significant changes upon SNX4 depletion (Fig. 5c, d). Additionally, the distribution of vesicles, grouped by bin size of 10 nm, showed no notable differences upon SNX4 depletion. (Supplementary Fig. 5). In SNX4 cKO synapses, the number of docked vesicles was significantly higher than in control (Fig. 5a, f) whilst the total number of vesicles was not altered (Fig. 5e). When normalized to the active zone length, the density of docked vesicles at the active zone length further increases by 50% in SNX4 cKO synapses compared to control (Fig. 5g). Moreover, we observed a significant decrease in active zone length, PSD length and vesicle cluster area (Fig. 5g-j). Together these data show that SNX4 depletion affects the presynaptic ultrastructure, characterized by smaller active zone length and vesicle cluster area, suggesting a decrease in overall synapse size. In these smaller synapses, SNX4 cKO neurons contain more docked synaptic vesicles leading to a substantially increased density of docked vesicles per release site.

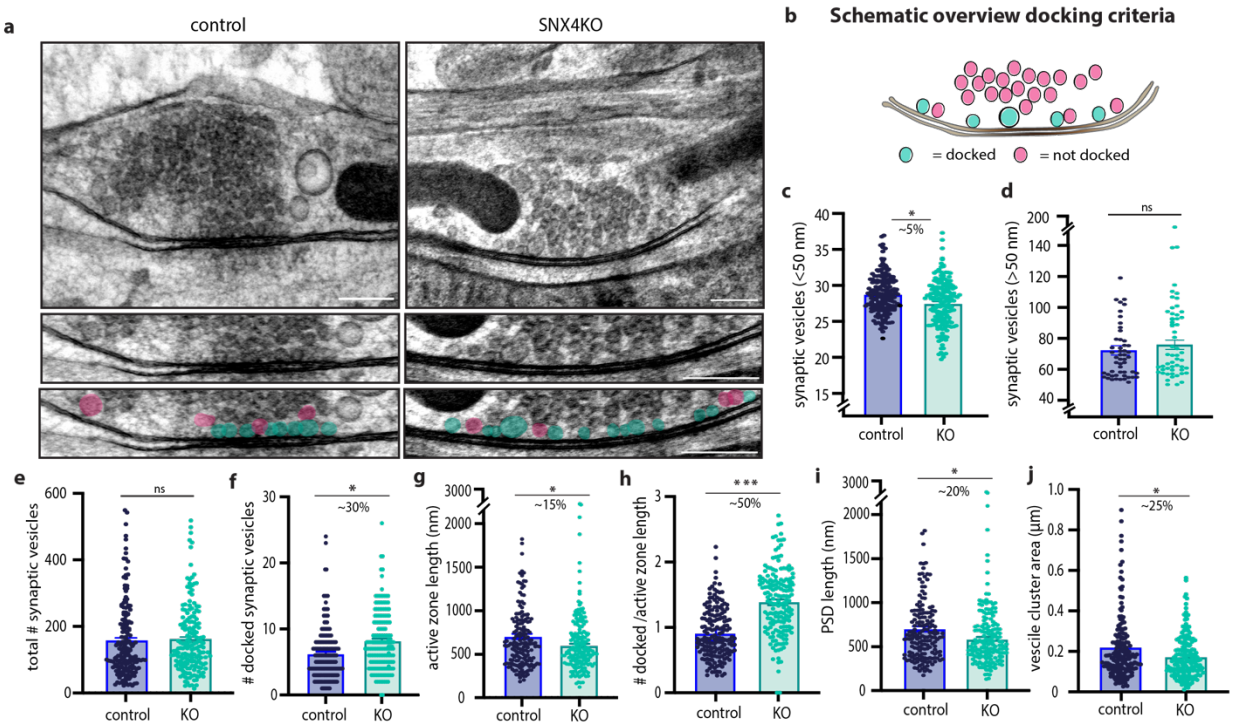

Figure 5: SNX4 depletion increases the number of docked vesicles at the active zone. (a) Example micrographs of control and SNX4 cKO synapses (Scale bar: 200 nm) with zoom in on the active zone region indicating docked (blue) and non-docked vesicles (pink) (Scale bar : 100 nm) **(b)** Schematic overview of docked and undocked vesicles. **(c & d)** The average vesicle size, distinguished between synaptic vesicles (<50 nm) and larger clear core vesicles (>50 nm). **(e)** The total amount of synaptic vesicles in the synaptic cloud. **(f)** The number of docked synaptic vesicles in control and SNX4 cKO synapses**. (g)** The active zone length. **(h)** The number of docked vesicles normalized to active zone length**. (i)** The post synaptic density (PSD) length. **(j)** The area of the vesicle cloud in control and SNX4 cKO synapses. Bar graphs represent mean with SEM with n = 174-175 synapses per group of N = 3 animals. Data points are individual synapses. ***p < 0.0001, **p < 0.001 using Mann-Whitney test.

Discussion

In this study we addressed the role of SNX4-dependent endosome sorting in synapses, using a new conditional SNX4 knock-out mouse model. We show that SNX4 cKO synapses elicit enhanced neurotransmission during train stimulation. SNX4 depletion did not affect vesicle recycling, basal autophagic flux or the levels and localization of SNARE-protein VAMP2/syb-2. Electron microscopy showed that synapses had an increased number of docked vesicles at the active zone, while the overall number of synaptic vesicles was normal. The active zone length was decreased upon SNX4 depletion, thereby further increasing the density of docked synaptic vesicles at the release site. Taken together, our data shows that the endosomal sorting protein SNX4 is a negative regulator of synaptic vesicle docking and release. These findings indicate that SNX4 regulates synaptic vesicle recruitment at the active zone.

Enhanced SV recruitment and increased SV docking explain increased transmission in SNX4 cKO synapses

SNX4 cKO synapses showed a 110% increase in neurotransmission during intense stimulation (Fig. 2f). A trend towards increased neurotransmission was observed already from the start of the train, and also in single evoked responses (Fig. 2c-d), but became more prominent (and significant) during sustained stimulation. Despite the variability within all datasets, both trends and the significant effect during sustained stimulation were fully reversed by acute SNX4 expression. The total number of synapses (Fig 1h) and fraction of active synapses (Fig 3g) was not affected in SNX4 cKO neurons, suggesting an intrasynaptic effect. While approximately twice more vesicles were released during sustained stimulation in the absence of SNX4 (Fig. 2f), our RRP estimation indicated a normal resting state RRP (Fig. 2i). All measures of release probability were normal (normal paired pulse facilitation, Fig. 2e, and shape of the rundown curve, Fig. 2f), indicating that an increased release probability is an unlikely explanation for the observed increase in neurotransmission during sustained stimulation. The mEPSC recordings were also not affected (Fig. 2k-m), this is consistent with the unaffected RRP estimate and single EPSC size and suggests that the observed increase in neurotransmission is not due to post-synaptic effects.

Hence, this suggests that a higher recruitment rate of SVs to the releasable pool (Fig. 2h, j) in SNX4 cKO synapses is responsible for the increased neurotransmission. While back extrapolation methods for estimating the RRP have their limitations (Neher, 2015) and mechanisms of SV recruitment remain not fully understood, it is evident that the involvement of newly recruited vesicles becomes more prominent during high frequency trains. In line with this, the increased neurotransmission of SNX4 cKO neurons was less prominent in 5Hz and 10Hz trains (Fig S2). Hence, an increased contribution of newly recruited vesicles during sustained stimulation is consistent with the fact that neurotransmission is increased especially during high frequency stimulation in SNX4 cKO synapses. No effects on neurotransmission were observed when overexpressing SNX4 on a control background, indicating that SNX4 is required but not rate limiting to limit synaptic release during prolonged stimulation.

The increase in neurotransmission during sustained stimulation was also observed with synaptic vesicle fusion reporter SypHy but not with the FM-64 dye. The latter method reports the release of only recycled vesicles, suggesting that these do not contribute significantly to the enhanced release. Finally, examining SV recycling with FM-64 dye indicates that the increased SV recruitment in SNX4 cKO synapses is not driven by an enhanced rate of the synaptic vesicle cycle, as endocytosis and release of recycled SVs were normal in SNX4 cKO synapses.

Ultrastructural characterization of SNX4 cKO synapses revealed a 50% increase in docked vesicles when normalized to active zone length. This increase might contribute to the

enhanced SV recruitment and increased neurotransmission observed in SNX4 cKO synapses. If more vesicles are already docked at the start of stimulation, they may on average be recruited faster during train stimulation. Synaptic vesicle docking is probably a dynamic equilibrium between various synaptic vesicle pools, modulated by activity (Kusick et al., 2020). However, an increase in docked SVs at the active zone also implies, on average, a closer proximity to calcium channels and therefore a higher release probability. However, measures of release probability were unaffected by SNX4 deficiency (as argued above) suggesting a normal channel coupling in SNX4 cKO synapses.

SNX4 at the crossroad of endosomal sorting and autophagy regulating synaptic output.

Increased neurotransmission upon depletion of endosomal genes has been shown by several labs (Fernandes et al., 2014; Soykan et al., 2021; Tagliatti et al., 2016; Uytterhoeven et al., 2011). These results are consistent with a postulated hypothesis that endosomes act sorting stations for SV proteins and control the balance between novel and reused SV proteins that affect SV release and neurotransmission efficiency (Fernandes et al., 2014; Truckenbrodt et al., 2018; Uytterhoeven et al., 2011).

In the presence of SNX4, the recycling process may lead to the re-use of older SV proteins that, as indirect consequence, potentially diminish the efficiency of SV exocytosis. In the absence of SNX4, older SV proteins are less recycled and traffic towards degradation, rendering the synapse with relatively more novel SV proteins, enhancing SV recruitment and fusion. Blocking the degradation pathway with HOPS/ESCRT mutants rescues the observed increased release(Fernandes et al., 2014; Uytterhoeven et al., 2011) . Similarly, Skywalker and ARF6 mutants show increased SV sorting through endosomal intermediates, increasing SV docking and release (Fernandes et al., 2014; Tagliatti et al., 2016; Uytterhoeven et al., 2011). Our data is consistent with this literature, demonstrating enhanced neurotransmission upon inactivation of an endosome sorting gene. That said, SNX4 cKO synapses do not show an accumulation of endosomal intermediates (Fig 5d) or decreased SV numbers (Fig 5e) as reported for other endosome gene mutants, marking a novel finding in endosomal protein knockout studies.

Endosomal sorting also mediates the delivery of active zone proteins, where disturbances in these pathways potentially correlate with smaller active zones and SVs, ultrastructural phenotypes we also observed in SNX4 cKO synapses. Previous studies suggest that the removal of SNX4 directs its cargo toward the degradative pathway (Hettema et al., 2003; Traer et al., 2007). Although the SNX4 cargo, particularly in mammalian neurons, is currently unknown, it is unlikely that VAMP2/syb-2 recycling explains our phenotype since the overall levels and localization of VAMP2/syb-2 remained unaffected upon SNX4 depletion.

Apart from endosome sorting, SNX4 has been reported to regulate several types of autophagy (Antón et al., 2020; Hanley et al., 2021; Zhou et al., 2022). Recent literature has shown that synaptic vesicle release could be regulated by synaptic autophagy (reviewed by Decet & Verstreken, 2021). Loss of ATG5 has been shown to result in increased neurotransmission, an effect independent from total SVs pool number (Kuijpers et al., 2021). We did not observe changes in total ATG5 levels upon SNX4 depletion, consistent with previous reports, (Antón et al., 2020), and no difference in basic autophagic flux of P62, contrasting with previous findings in HeLa cells (Antón et al., 2020). This suggests that SNX4 may have a specialized role in neurons, that regulates synaptic transmission independent of autophagic flux by a yet-to-be determined mechanism.

352 **SNX-BAR proteins critical for synapse function.**
353
354 Many of our examined synaptic parameters remained unaltered or showed considerable
355 variability, including our hypothesis that depletion of a synaptic endosomal sorting protein
356 would disrupt synaptic recycling. This suggests the presence of redundant pathways
357 compensating for SNX4 depletion, potentially involving other SNX-BAR complexes or
358 endosomal sorting complexes like ESCPE, retriever, or retromer (Simonetti et al., 2023).
359 Particularly SNX-BAR proteins, such as SNX7 and SNX30, are of potential interest for future
360 research due to their ability to form selective complexes with SNX4 (Antón et al., 2020). The
361 role of endosome sorting in the synaptic vesicle cycle is increasingly recognized through
362 knockout studies targeting various endosomal complexes, revealing changes in SV exocytosis,
363 SV endocytosis, or endosome-like vesicle numbers (X. Chen et al., 2017; X. W. Chen et al.,
364 2008; Inoshita et al., 2017; Tagliatti et al., 2016). Our data supports this, showing for the first
365 time that a protein from the highly evolutionary conserved SNX-BAR protein family, such as
366 SNX4, regulates SV docking at the active zone and sustained SV release. Taken together, we
367 show that endosomal sorting protein SNX4 regulates synaptic vesicles recruitment at the active
368 zone. The precise regulation of vesicle availability is crucial for a synapse to effectively
369 coordinate neurotransmission, a process heavily relying on endosome sorting mechanisms.
370
371
372
373 **MATERIAL&METHODS**
374
375 **Laboratory animals and SNX4 cKO generation**
376
377 Animals were housed and bred according to institutional and Dutch governmental guidelines
378 (DEC-FGA 11-03 and AVD112002017824). The SNX4 conditional KO targeting strategy
379 aimed to achieve mouse SNX4 gene loss of function by flanking exon 3 and 4 with loxP sites
380 to acutely remove these exons by Cre recombinase (Fig 1a). In the targeting vector, self-
381 deletion anchor sites flank the Neomycin cassette, and Diphtheria toxin A fragment (DTA) is
382 used for negative selection. Mouse genomic fragments containing homology arms were
383 amplified from a BAC clone using high-fidelity Taq DNA polymerase. These fragments were
384 then sequentially assembled into a targeting vector along with the recombination sites and
385 selection markers. Homologously targeted $SNX4^{lox}$ embryonic stem cells (C57BL/6) were
386 injected into blastocysts and implanted into pseudopregnant females to produce germ-line
387 chimeras, which were mated with inbred C57BL/6 mice. The mouse colony was maintained
388 by homozygous lox/lox mice breeding, with every third or fourth generation mice were
389 backcrossed with C57BL/6 mice. The following primers were used for genotyping: forward
390 primer: TTCTTGAGGGTAACAGAAATCCTTAGTGCC and reverse primer
391 CTCTGAATACCAGGAGAGTCCACAAGAGC.
392
393
394 **Primary neuronal cultures**
395
396 Dissociated hippocampal neuron cultures were prepared from P01 SNX4KO mouse embryos.
397 Hippocampi dissected free of meninges in Hanks' balanced salt solution (Sigma, H9394)
398 supplemented with 10 mM HEPES (Gibco, 15630- 056). The hippocampi were isolated from
399 the tissue and digested with 0.25% trypsin (Gibco, 15090-046) in Hanks' HEPES for 20 min
400 at 37°C. Hippocampi were washed three times with Hanks' HEPES and triturated with fire-
401 polished glass pipettes. Neurons were counted and plated in Neurobasal medium (Gibco,

402 21103-049) supplemented with 2% B-27 (Gibco, 17504-044), 1.8% HEPES, 0.25% Glutamax
403 (Gibco, 35050-038), and 0.1% penicillin–streptomycin (Gibco, 15140-122). Hippocampal
404 neurons were plated in 12-well plates at a density of 25.000 cells per well on 18-mm glass
405 coverslips containing rat glia or 50.000 cells on coverslips containing 0.01% Poly-ornithin
406 (Sigma P4957) and 2.5 ug/ml laminin coating (Sigma L2020) solution o/n at RT. Neuronal
407 cultures were kept in supplemented Neurobasal at 37°C and 5% CO2 until DIV21.
408
409 **Constructs and lentiviral infection**
410
411 Neuronal cultures were infected with EGFP-Cre and EGFP-control (delta Cre) at DIV0 to
412 generate SNX4KO. All constructs were cloned into lentiviral vectors under the synapsin
413 promoter, and lentiviral particles were generated following the protocol previously described
414 in (Naldini et al., 1996).The presence of an EGFP nuclear localization sequence (NLS) allowed
415 identification of tranduced cells (Kaeser et al., 2011). For synaptic vesicle release experiments,
416 neurons were infected with Synaptophysin-pHluorin lentivirus at DIV7. Titration of lentiviral
417 particle batches was performed by assessment of number of fluorescent cells upon infection to
418 ensure 100% infection efficiency. For rescue experiments and SNX4 overexpression
419 experiments a lentiviral construct of mouse SNX4 was generated with an ECFP fluorescent tag
420 together with an 2A cleavage site in between in a FUW backbone (pECFP-T2A-SNX4(mus
421 musculus)- FUW).
422
423 **Western blot**
424
425 Cortical neurons at DIV21 were washed with phosphate-buffered saline (PBS) and lysed in
426 Laemmli sample buffer consisting of 2% SDS (VWR chemicals, M107), 10% glycerol (Merck,
427 818709), 0.26 M b-mercaptoethanol (Sigma, M3148), 60 mM Tris-HCl (Serva, 37180) pH 6.8,
428 and 0.01% Bromophenol blue (Applichem, A3640). Samples of 450.000 neurons run in SDS-
429 PAGE (10% 1 mm acrylamide gel with 2, 2, 2-Trichloroethanol) using standard SDS-PAGE
430 technique and transferred into polyvinylideenfluoride membranes (Bio-rad) (1 hour, 0.25 mA,
431 4 C°). Blots were blocked and incubated with primary antibodies (4 degrees O/N) in PBS
432 containing 0.1% Tween-20 (Sigma, P2287) (PBS-T) and 5% milk. Primary antibodies included
433 polyclonal rabbit SNX4 (1:500; SySy, Cat. No. 392 003), monoclonal mouse actin (1:10000;
434 Chemicon, Cat. No. MAB1501), monoclonal mouse VAMP2/synaptobrevin2 (1:2000; SySy,
435 CL 69.1), and polyclonal rabbit BACE-1 (1:500; Abcam ab20770). After washing with PBS-
436 T, blots were incubated with secondary horseradish peroxidase (HRP)-labeled antibodies
437 (1:10000; Sigma) in PBS-T and 5% milk (1 hour, RT). After washing with PBS-T, blots were
438 developed with SuperSignal West Femto substrate (Thermo Scientific, 11859290) for 2 min.
439 Chemiluminescence labelled proteins were visualised with the Odyssey Imaging System (LI-
440 COR) for appropriate times and analysed with Image Studio 5.2 software (LI-COR) or ImageJ.
441 A fixed region of interest (ROI) was used to measure the average intensity, which was then
442 normalized to 1) the loading control (housekeeping genes Actin or GAPDH) and 2) the control
443 within each independent experiment (N) to account for weekly variations.
444
445 **Immunocytochemistry**
446
447 Neurons at DIV21 were fixed in 3.7% formaldehyde (Electron Microscopies Sciences, 15680)
448 in PBS, pH 7.4, for 25 min at RT. After washing with PBS, cells were permeabilized for 5 min
449 with 0.5% Triton X- 100 (Fisher Chemical, T/3751/08)–PBS and incubated for 30 min with
450 PBS containing 2% normal goat serum (Gibco, 16210-072) and 0.1% Triton X-100 to block
451 nonspecific binding. Incubations with primary antibodies were performed O/N at 4°C. After

452 PBS washing steps incubations with secondary antibodies followed for 1h at RT. Primary
453 antibodies included polyclonal rabbit SNX4 (1:500; SySy, Cat. No. 392 003), monoclonal
454 mouse VAMP2/synaptobrevin2 (1:1000; SySy, CL 69.1), and polyclonal chicken MAP2
455 (1:300; Abcam ab5392) and Alexa Fluor conjugated secondary antibodies (1:1000;
456 Invitrogen). Coverslips were mounted with Dabco-Mowiol 4-88 (Sigma, 81381) and confocal
457 microscope (Nikon eclipse Ti) using a 40× oil immersion objective (NA = 1.3)) was used to
458 examine the samples. Laser settings were kept constant within experimental conditions.

459 **Electrophysiological recordings**

460 Autaptic cultures of *SNX4* null neurons were grown for 21–25 days before measuring. Whole-
461 cell voltage-clamp recordings (V_m = −70 mV) were performed at room temperature with
462 borosilicate glass pipettes (2.5–4.5 mOhm) filled with 136 mM KCl, 17.8 mM HEPES, 0.6
463 mM $MgCl_2$, 4 mM ATP-Mg, 0.3 mM GTP-Na, 12 mM phosphocreatine dipotassium salt, 45.3
464 mM phosphocreatine kinase, and 1 mM EGTA (pH 7.30). External solution contained the
465 following (in mM): 10 HEPES, 10 glucose, 140 NaCl, 2.4 KCl, 4 $MgCl_2$, and 4 $CaCl_2$ (pH =
466 7.30, 300 mOsmol). Recording was acquired with an MultiClamp 700B amplifier (Molecular
467 Devices), Digidata 1550B, and Clampex 9.0 software (Molecular Devices). After whole-cell
468 mode was established, only cells with an access resistance of < 15 MΩ and leak current of <
469 300 pA were accepted for analysis. Serie resistance compensation was between 70-80%.
470 Access resistance was measured before and after recordings. Recordings with a > 20% increase
471 in access resistance were excluded from analysis, as well as recordings that showed voltage
472 clamp escape or clipping. GABAergic recordings were identified based on their postsynaptic decay
473 kinetics and excluded. EPSCs were elicited by a 1-ms depolarization to 30 mV. Offline analysis
474 was performed with MATLAB R2019a (Mathworks) using custom-written software routines
475 (viewEPSC, downloaded from user vhuson on Github on 13 Sept 2023). RRP and slope estimates
476 were obtained by a linear fit of cumulative total charge plot from pulse 80 to 100 for each
477 individual cell with y-intercept for RRP estimate and slope as recruitment rate estimate
478 (Schneggenburger et al., 1999).

479 **Live cell imaging**
480
481 Live imaging experiments were performed at DIV21 on a custom build imaging microscope
482 (IX81; Olympus) with an MT20 light source (Olympus) with a 40× oil objective (NA=1.3)
483 appropriate filter sets (semrock, Rochester, NY) and an EM charge-coupled device camera
484 (C9100-02; Hamamatsu Photonics, Japan). Xcellence RT imaging software (Olympus)
485 controlled the microscope and image acquisition. Coverslips were perfused with Tyrode's
486 solution (119 mM NaCl, 2.5 mM KCl, 2 mM $CaCl_2^-$ 2H2O, 2mM $MgCl_2^-$ 6H2O, 25 mM
487 HEPES, and 30 mM glucoseH2O, pH 7.4, mOsmol 280). For synaptic vesicle release
488 experiments, time-lapse (2 Hz) recordings consisted of 30 s baseline recordings followed by
489 two electrical field stimulations with 60s recovery time in between and a final stimulation 10s
490 of NH4-Tyrode's perfusion (2 mM CaCl2, 2.5 mM KCl, 119 mM NaCl, 2 mM MgCl2, 30 mM
491 glucose, 25 mM HEPES, 50 mN NH4Cl at pH 7.4). Electrical field stimulation was applied via
492 parallel platinum electrodes powered by a stimulus isolator (WPI A385) delivering 30-mA, 1-
493 ms pulses, regulated by a Master-8 pulse generator (A.M.P.I.) providing 100 APs at 40 Hz with
494 a 0.5-s interval. Glass capillaries close to the isolated neuron were used for chemical
495 stimulation. For the FM4-64 experiments, neurons were pre imaging incubated in high
496 potassium Tyrode's for 10 min at 37 C°(61.5 mM NaCl, 60 mM KCl, 2 mM CaCl22H2O,
497 2mM MgCl2 6H2O, 25 mM HEPES and 30 mM glucoseH2O, pH 7.4, mOsmol 280).
498

499
500 **Imaging analysis**
501
502 For live-cell imaging analysis, timelapse recordings stacks were used to analyze SyPhy and
503 FM4-64 fusion events (2 Hz, 1000 × 1000pixels). In ImageJ fusion events were selected
504 manually and fluorescence traces were measured in a circular 3 × 3 pixel ROI (0.6 x 0.6 um),
505 somatic events not included. ROI intensity measures of SyPhy puncta were exported to a
506 custom-built Matlab program for semiautomated detection of fusion events and duration (Moro
507 et al., 2021). Fluorescence traces from the ROI were expressed as fluorescence change (deltaF)
508 compared to initial fluorescence (F0), with the average of frames 1-10 for determining F0.
509 Fusion events were automatically detected when displaying a sudden increase of two standard
510 deviations above F0. Synaptic vesicle pool numbers and synapses were estimated using MAP2
511 mask in automated image analysis software SynD (Schmitz et al., 2011). Active synapses were
512 determined by 3x SD over baseline. Synapse detection settings were optimized to measure
513 SyPhy and VAMP2/syb-2 puncta signal and kept constant within the same dataset. For FM4-
514 64 puncta, fluorescence traces were expressed as change (DF) compared to baseline
515 fluorescence (F0) and the average of the last 10 frames was used to determine the maximum
516 FM4-64 release.
517 For fixed cell imaging analysis, VAMP2 puncta number within MAP2 mask were
518 analysed using automated SynD software (see above). For sholl analysis, dendrite mask based
519 on MAP2 staining was used to either determine the number of dendritic branches per shell or
520 average VAMP2 intensity within the neurite mask.

521 **Cryofixation electron microscopy**

522 Dissociated hippocampal neurons (5000 k/well) from SNX4 cKO mice were plated on pre-
523 grown cultures of rat glia on sapphire disks (Wohlwend GmbH) to form micro-networks of 2–
524 10 neurons per sapphire disk. Prior to cell culture, sapphire disks were etched for 30 minutes
525 in 60% sulfuric acid, washed, incubated in 3M KOH overnight, washed and dried before carbon
526 coating and subsequent baking at 180 C for 2 hours. Sapphire discs were coated by a mixture
527 of 0.1 mg/ml poly-d-lysine (Sigma), 0.7 mg/ml rat tail collagen (BD Biosciences), and 10 mM
528 acetic acid (Sigma) and placed in an agarose-coated 12-well plate to form glia monolayer
529 islands selectively on sapphire disks. The sapphire disks were cryofixed in an EM-PACT2
530 (Leica Microsystems) high-pressure freezer in 5% trehalose/10% BSA in 0.05M phosphate
531 buffer pH 7.4 320 mOsm cryoprotectant. Frozen samples were postfixed in 1% OsO4/ 5%
532 saturated K4Fe(CN)6 in H2O in acetone at −90°C for 74 hours and brought to 0°C at 5°/h.
533 After a couple washes with ice-cold acetone, the sapphire disks were washed with propylene
534 oxide and with an increasing Epon concentration series. The samples were embedded in fresh
535 Epon overnight and left to polymerize at 65°C for 48 h. Sapphire disks were separated from
536 the Epon by dipping the samples in boiling water and liquid nitrogen and regions with micro-
537 networks were selected by light microscopy. These regions were cut out and mounted on pre-
538 polymerized Epon blocks for ultrathin sectioning. Ultrathin sections (80 nm) were cut parallel
539 to the sapphire disk, collected on single-slot, formvar-coated copper grids, and stained in uranyl
540 acetate and lead citrate. Hippocampal synapses were randomly selected at low magnification
541 using an electron microscope (JEOL1010), and the conditions were blinded. For each
542 condition, the number of docked SVs, total SV number, and active zone length were measured
543 on digital images taken at 80,000-fold magnification using custom-written semiautomatic
544 image analysis software running in Matlab (Mathworks). For all morphological analyses the
545 following requirements were set: clearly recognizable synapses with intact synaptic plasma
546 membranes with a recognizable pre- and postsynaptic area and defined SV membranes. SVs

were defined as docked if there was no distance visible between the SV membrane and the active zone membrane (pixel size 0.6505 nm).

Statistics

Data are shown as mean +- SEM. Data that violated both normality (Shapiro-Wilk) and homogeneity (Levene test) was tested with the two-sided Mann–Whitney U test. Data exhibiting a normal distribution yet significantly altered variation were tested with Welch's t-test. When assumptions of homogeneity and normality were met, data were tested with Student's t test or one-way ANOVA with Tukey's multiple comparisons test. For the analysis of electron microscopy data, electrophysiology data and live cell imaging (pHluorin and FM dye), the intraclass correlation coefficient (ICC) was calculated for different variables applicable to each experiment such as culture batch, sapphire or synapse originating from the same neuron. If ICC was close to 0.1 or above, indicating that a considerable portion of the total variance can be attributed to e.g. culture week, multilevel analysis was performed to accommodate nested data (Aarts et al., 2014). For electrophysiology data, we excluded outliers beyond mean ± 3xSD. Bar graphs were plotted as the mean with SEM, where individual data points represent fields of view, neurons or synapses (EM data set).

Acknowlegdements

The authors thank dr. Sander Groffen for help with the conditional knock-out mouse design, Joke Wortel for housing and breeding the mice, Desiree Schut for helping with neuronal cultures, Robbert Zalm for cloning and lentiviral production, Marien P Dekker for assistance with EM analysis. We thank Jill Gerritsen for electrophysiology data analysis. We would like to thank Elise van Bree and Sonia Vazquez-Sanchez for their pioneering work on synaptic release in SNX4 shRNA models. The van Weering lab is supported by Alzheimer Nederland (WE.03-2019-06).

Author contributions

J.P. performed experiments and analyzed the data. N.J.B. and L.N.C collected and analyzed Ephys data. J.R.T.vW collected and analyzed EM data. J.P., M.V. and J.R.T.vW designed the experiments and wrote the manuscript with input of all authors.

References

Aarts, E., Verhage, M., Veenvliet, J. V., Dolan, C. V., & Van Der Sluis, S. (2014). A solution to dependency: using multilevel analysis to accommodate nested data. *Nature Neuroscience*, *17*(4), 491–496. https://doi.org/10.1038/NN.3648

Antón, Z., Betin, V. M. S., Simonetti, B., Traer, C. J., Attar, N., Cullen, P. J., & Lane, J. D. (2020). A heterodimeric SNX4–SNX7 SNX-BAR autophagy complex coordinates ATG9A trafficking for efficient autophagosome assembly. *Journal of Cell Science*, *133*(14). https://doi.org/10.1242/jcs.246306

Carlton, J., Bujny, M., Rutherford, A., & Cullen, P. (2005). Sorting nexins--unifying trends and new perspectives. *Traffic (Copenhagen, Denmark)*, *6*(2), 75–82. https://doi.org/10.1111/J.1600-0854.2005.00260.X

Ceccarelli, B., Hurlbut, W. P., & Mauro, A. (1973). Turnover of Transmitter and Synaptic Vesicles at the Frog Neuromuscular Junction. *Journal of Cell Biology*, *57*(2), 499–524. https://doi.org/10.1083/JCB.57.2.499

589 Chen, X., Ma, W., Zhang, S., Paluch, J., Guo, W., & Dickman, D. K. (2017). The
590 BLOC-1 Subunit Pallidin Facilitates Activity-Dependent Synaptic Vesicle
591 Recycling. *Eneuro*, *4*(1), ENEURO.0335-16.2017.
592 https://doi.org/10.1523/ENEURO.0335-16.2017
593 Chen, X. W., Feng, Y. Q., Hao, C. J., Guo, X. L., He, X., Zhou, Z. Y., Guo, N., Huang,
594 H. P., Xiong, W., Zheng, H., Zuo, P. L., Zhang, C. X., Li, W., & Zhou, Z. (2008).
595 DTNBP1, a schizophrenia susceptibility gene, affects kinetics of transmitter
596 release. *Journal of Cell Biology*, *181*(5), 791–801.
597 https://doi.org/10.1083/jcb.200711021
598 Cullen, P. J., & Steinberg, F. (2018). To degrade or not to degrade: mechanisms and
599 significance of endocytic recycling. *Nature Reviews Molecular Cell Biology*,
600 *19*(11), 679–696. https://doi.org/10.1038/s41580-018-0053-7
601 Decet, M., & Verstreken, P. (2021). Presynaptic Autophagy and the Connection With
602 Neurotransmission. *Frontiers in Cell and Developmental Biology*, *9*.
603 https://doi.org/10.3389/FCELL.2021.790721
604 Dörrbaum, A. R., Kochen, L., Langer, J. D., & Schuman, E. M. (2018). Local and global
605 influences on protein turnover in neurons and glia. *ELife*, *7*.
606 https://doi.org/10.7554/ELIFE.34202
607 Fernandes, A. C., Uytterhoeven, V., Kuenen, S., Wang, Y.-C., Slabbaert, J. R., Swerts,
608 J., Kasprowicz, J., Aerts, S., & Verstreken, P. (2014). Reduced synaptic vesicle
609 protein degradation at lysosomes curbs TBC1D24/sky-induced neurodegeneration.
610 *The Journal of Cell Biology*, *207*(4), 453–462.
611 https://doi.org/10.1083/jcb.201406026
612 Granseth, B., Odermatt, B., Royle, S. J. J., & Lagnado, L. (2006). Clathrin-mediated
613 endocytosis is the dominant mechanism of vesicle retrieval at hippocampal
614 synapses. *Neuron*, *51*(6), 773–786.
615 https://doi.org/10.1016/J.NEURON.2006.08.029
616 Hanley, S. E., Willis, S. D., & Cooper, K. F. (2021). Snx4-assisted vacuolar targeting of
617 transcription factors defines a new autophagy pathway for controlling ATG
618 expression. *Autophagy*, *17*(11), 3547.
619 https://doi.org/10.1080/15548627.2021.1877934
620 Hettema, E. H., Lewis, M. J., Black, M. W., & Pelham, H. R. B. (2003). Retromer and
621 the sorting nexins Snx4/41/42 mediate distinct retrieval pathways from yeast
622 endosomes. *EMBO Journal*, *22*(3), 548–557. https://doi.org/10.1093/emboj/cdg062
623 Heuser, E., & Reese, T. S. (1973). Evidence for Recycling of Synaptic Vesicle
624 Membrane during Transmitter Release at the Frog Neuromuscular Junction. *The*
625 *Journal of Cell Biology*, *57*, 15–344.
626 Huotari, J., & Helenius, A. (2011). Endosome maturation. *The EMBO Journal*, *30*(17),
627 3481–3500. https://doi.org/10.1038/EMBOJ.2011.286
628 Inoshita, T., Arano, T., Hosaka, Y., Meng, H., Umezaki, Y., Kosugi, S., Morimoto, T.,
629 Koike, M., Chang, H.-Y., Imai, Y., & Hattori, N. (2017). Vps35 in cooperation
630 with LRRK2 regulates synaptic vesicle endocytosis through the endosomal
631 pathway in Drosophila. *Human Molecular Genetics*, *26*(15), 2933–2948.
632 https://doi.org/10.1093/hmg/ddx179
633 Kaeser, P. S., Deng, L., Wang, Y., Dulubova, I., Liu, X., Rizo, J., & Südhof, T. C.
634 (2011). RIM proteins tether Ca2+ channels to presynaptic active zones via a direct
635 PDZ-domain interaction. *Cell*, *144*(2), 282–295.
636 https://doi.org/10.1016/j.cell.2010.12.029
637 Kim, N. Y., Cho, M. H., Won, S. H., Kang, H. J., Yoon, S. Y., & Kim, D. H. (2017).
638 Sorting nexin-4 regulates β-amyloid production by modulating β-site-activating

cleavage enzyme-1. *Alzheimer's Research and Therapy*, *9*(1), 4. https://doi.org/10.1186/s13195-016-0232-8

Kononenko, N. L., & Haucke, V. (2015). Molecular mechanisms of presynaptic membrane retrieval and synaptic vesicle reformation. In *Neuron* (Vol. 85, Issue 3, pp. 484–496). Cell Press. https://doi.org/10.1016/j.neuron.2014.12.016

Kuijpers, M., Kochlamazashvili, G., Stumpf, A., Puchkov, D., Swaminathan, A., Lucht, M. T., Krause, E., Maritzen, T., Schmitz, D., & Haucke, V. (2021). Neuronal Autophagy Regulates Presynaptic Neurotransmission by Controlling the Axonal Endoplasmic Reticulum. *Neuron*, *109*(2), 299-313.e9. https://doi.org/10.1016/J.NEURON.2020.10.005

Kusick, G. F., Chin, M., Raychaudhuri, S., Lippmann, K., Adula, K. P., Hujber, E. J., Vu, T., Davis, M. W., Jorgensen, E. M., & Watanabe, S. (2020). Synaptic vesicles transiently dock to refill release sites. *Nature Neuroscience 2020 23:11*, *23*(11), 1329–1338. https://doi.org/10.1038/s41593-020-00716-1

Ma, M., Burd, C. G., & Chi, R. J. (2017). Distinct complexes of yeast Snx4 family SNX-BARs mediate retrograde trafficking of Snc1 and Atg27. *Traffic (Copenhagen, Denmark)*, *18*(2), 134. https://doi.org/10.1111/TRA.12462

Moro, A., van Nifterick, A., Toonen, R. F., & Verhage, M. (2021). Dynamin controls neuropeptide secretion by organizing dense-core vesicle fusion sites. *Science Advances*, *7*(21), 659–680. https://www.science.org/doi/10.1126/sciadv.abf0659

Naldini, L., Blömer, U., Gallay, P., Ory, D., Mulligan, R., Gage, F. H., Verma, I. M., & Trono, D. (1996). In Vivo Gene Delivery and Stable Transduction of Nondividing Cells by a Lentiviral Vector. *Science*, *272*(5259), 263–267. https://doi.org/10.1126/SCIENCE.272.5259.263

Neher, E. (2015). Merits and Limitations of Vesicle Pool Models in View of Heterogeneous Populations of Synaptic Vesicles. *Neuron*, *87*(6), 1131–1142. https://doi.org/10.1016/J.NEURON.2015.08.038

Rizzoli, S. O. (2014). Synaptic vesicle recycling: steps and principles. *The EMBO Journal*, *33*(8), 788. https://doi.org/10.1002/EMBJ.201386357

Sardana, R., & Emr, S. D. (2021). Membrane Protein Quality Control Mechanisms in the Endo-Lysosome System. *Trends in Cell Biology*, *31*(4), 269–283. https://doi.org/10.1016/J.TCB.2020.11.011

Schmitz, S. K., Hjorth, J. J. J., Joemai, R. M. S., Wijntjes, R., Eijgenraam, S., de Bruijn, P., Georgiou, C., de Jong, A. P. H., van Ooyen, A., Verhage, M., Cornelisse, L. N., Toonen, R. F., & Veldkamp, W. (2011). Automated analysis of neuronal morphology, synapse number and synaptic recruitment. *Journal of Neuroscience Methods*, *195*(2), 185–193. https://doi.org/10.1016/J.JNEUMETH.2010.12.011

Schneggenburger, R., Meyer, A. C., & Neher, E. (1999). Released fraction and total size of a pool of immediately available transmitter quanta at a calyx synapse. *Neuron*, *23*(2), 399–409. https://doi.org/10.1016/S0896-6273(00)80789-8

Schoch, S., Deák, F., Königstorfer, A., Mozhayeva, M., Sara, Y., Südhof, T. C., & Kavalali, E. T. (2001). SNARE function analyzed in synaptobrevin/VAMP knockout mice. *Science*, *294*(5544), 1117–1122. https://doi.org/10.1126/SCIENCE.1064335/SUPPL_FILE/1064335S2_THUMB.GIF

Simonetti, B., Daly, J. L., & Cullen, P. J. (2023). Out of the ESCPE room: Emerging roles of endosomal SNX-BARs in receptor transport and host–pathogen interaction. *Traffic*, *24*(6), 234–250. https://doi.org/10.1111/TRA.12885

687 Soykan, T., Haucke, V., & Kuijpers, M. (2021). Mechanism of synaptic protein turnover
688 and its regulation by neuronal activity. *Current Opinion in Neurobiology*, *69*, 76–
689 83. https://doi.org/10.1016/J.CONB.2021.02.006
690 Südhof, T. C. (2000). The synaptic vesicle cycle revisited. *Neuron*, *28*(2), 317–320.
691 https://doi.org/10.1016/S0896-6273(00)00109-4
692 Sugatha, J., Priya, A., Raj, P., Jaimon, E., Swaminathan, U., Jose, A., Pucadyil, T. J., &
693 Datta, S. (2023). Insights into cargo sorting by SNX32 and its role in neurite
694 outgrowth. *ELife*, *12*. https://doi.org/10.7554/eLife.84396
695 Tagliatti, E., Fadda, M., Falace, A., Benfenati, F., & Fassio, A. (2016). Arf6 regulates
696 the cycling and the readily releasable pool of synaptic vesicles at hippocampal
697 synapse. *ELife*, *5*(JANUARY2016), 1–18. https://doi.org/10.7554/eLife.10116
698 Teasdale, R. D., Loci, D., Houghton, F., Karlsson, L., & Gleeson, P. A. (2001). A large
699 family of endosome-localized proteins related to sorting nexin 1. *The Biochemical*
700 *Journal*, *358*(Pt 1), 7–16. https://doi.org/10.1042/0264-6021:3580007
701 Toh, W. H., Cheryl Chia, P. Z., Iqbal Hossain, M., & Gleeson, P. A. (2018). GGA1
702 regulates signal-dependent sorting of BACE1 to recycling endosomes, which
703 moderates Aβ production. *Molecular Biology of the Cell*, *29*(2), 191.
704 https://doi.org/10.1091/MBC.E17-05-0270
705 Traer, C. J., Rutherford, A. C., Palmer, K. J., Wassmer, T., Oakley, J., Attar, N., Carlton,
706 J. G., Kremerskothen, J., Stephens, D. J., & Cullen, P. J. (2007). SNX4 coordinates
707 endosomal sorting of TfnR with dynein-mediated transport into the endocytic
708 recycling compartment. *Nature Cell Biology*, *9*(12), 1370–1380.
709 https://doi.org/10.1038/ncb1656
710 Truckenbrodt, S., Viplav, A., Jähne, S., Vogts, A., Denker, A., Wildhagen, H.,
711 Fornasiero, E. F., & Rizzoli, S. O. (2018). Newly produced synaptic vesicle
712 proteins are preferentially used in synaptic transmission. *The EMBO Journal*,
713 *37*(15), 1–24. https://doi.org/10.15252/embj.201798044
714 Uytterhoeven, V., Kuenen, S., Kasprowicz, J., Miskiewicz, K., & Verstreken, P. (2011).
715 Loss of Skywalker reveals synaptic endosomes as sorting stations for synaptic
716 vesicle proteins. *Cell*, *145*(1), 117–132. https://doi.org/10.1016/j.cell.2011.02.039
717 Van Weering, J. R. T., Sessions, R. B., Traer, C. J., Kloer, D. P., Bhatia, V. K., Stamou,
718 D., Carlsson, S. R., Hurley, J. H., & Cullen, P. J. (2012). Molecular basis for SNX-
719 BAR-mediated assembly of distinct endosomal sorting tubules. *EMBO Journal*,
720 *31*(23), 4466–4480. https://doi.org/10.1038/emboj.2012.283
721 van Weering, J. R. T., Verkade, P., & Cullen, P. J. (2012). SNX–BAR-Mediated
722 Endosome Tubulation is Co-ordinated with Endosome Maturation. *Traffic*, *13*(1),
723 94–107. https://doi.org/10.1111/J.1600-0854.2011.01297.X
724 Vazquez-Sanchez, S., Gonzalez-Lozano, M. A., Walfenzao, A., Li, K. W., & van
725 Weering, J. R. T. (2020). The endosomal protein sorting nexin 4 is a synaptic
726 protein. *Scientific Reports*, *10*(1). https://doi.org/10.1038/s41598-020-74694-6
727 Vietri, M., Radulovic, M., & Stenmark, H. (2020). The many functions of ESCRTs.
728 *Nature Reviews. Molecular Cell Biology*, *21*(1), 25–42.
729 https://doi.org/10.1038/S41580-019-0177-4
730 Watanabe, S., & Boucrot, E. (2017). Fast and ultrafast endocytosis. *Current Opinion in*
731 *Cell Biology*, *47*, 64–71. https://doi.org/10.1016/J.CEB.2017.02.013
732 Watanabe, S., Rost, B. R., Camacho-Pérez, M., Davis, M. W., Söhl-Kielczynski, B.,
733 Rosenmund, C., & Jorgensen, E. M. (2013). Ultrafast endocytosis at mouse
734 hippocampal synapses. *Nature*, *504*(7479), 242–247.
735 https://doi.org/10.1038/nature12809

Zhou, C., Wu, Z., Du, W., Que, H., Wang, Y., Ouyang, Q., Jian, F., Yuan, W., Zhao, Y., Tian, R., Li, Y., Chen, Y., Gao, S., Wong, C. C. L., & Rong, Y. (2022). Recycling of autophagosomal components from autolysosomes by the recycler complex. *Nature Cell Biology 2022 24:4*, *24*(4), 497–512. https://doi.org/10.1038/s41556-022-00861-8

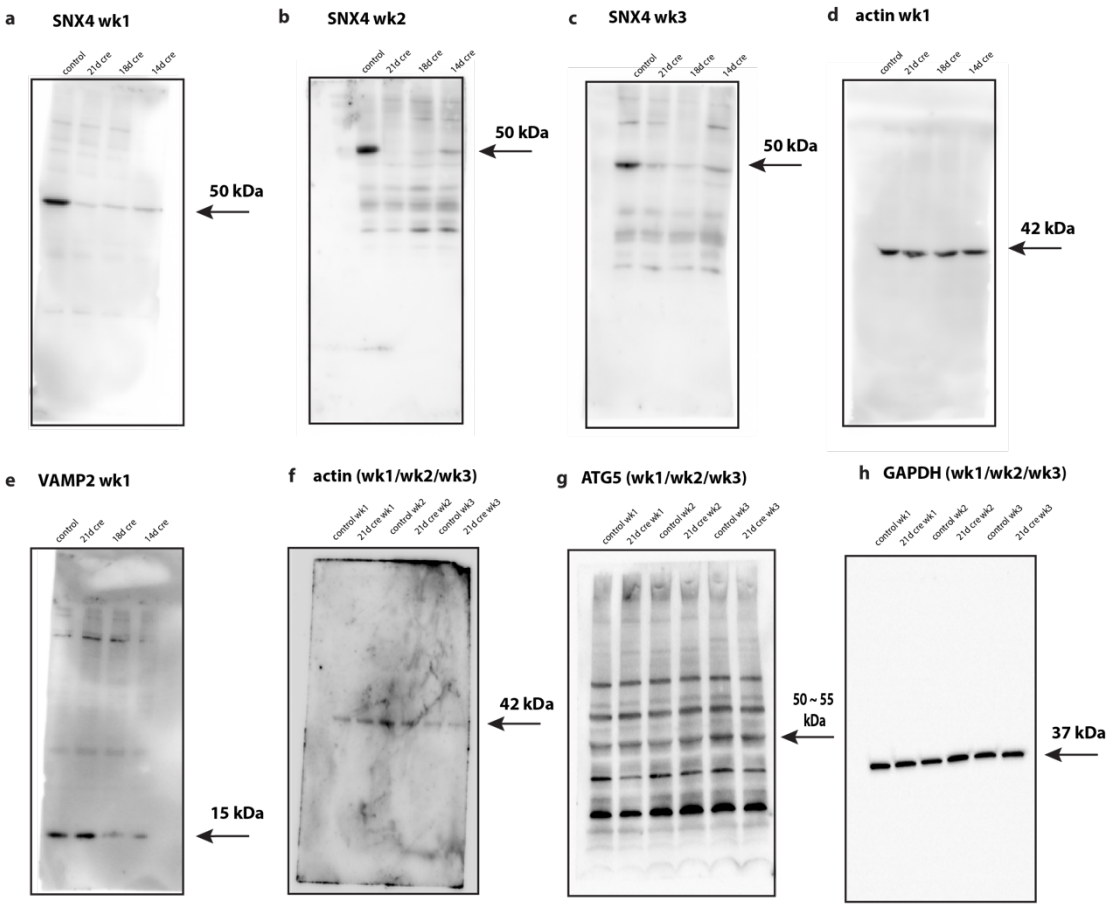

Supplementary figure 1: Overview of uncropped blots used for western blot analysis. (a,b,c) SNX4 at 50 kDa for control (21 days of dcre), 21 days of cre, 18 days of cre and 14 days of cre. Repeated for three different animals, wk1 is normalized to actin and wk2 and wk3 are normalized to unspecific band on the blot. Fold of change is determined for all weeks by normalizing to control per week. **(d)** Actin at 42 kDa for control, 21 days of cre, 18 days of cre and 14 days of cre. Same animal and transfer as SNX4 wk1. **(e)** VAMP2 at 15 kDa for control, 21 days of cre, 18 days of cre and 14 days of cre. Same animal and transfer as SNX4 wk1. **(f)** Actin at 42 kDa for control and 21 days of cre for three different animals on one blot. (**g)** ATG5 at 55bkDa for control and 21 days of cre for three different animals on one blot. (**h)** GAPDH at 42 kDa for control and 21 days of cre for three different animals on one blot.

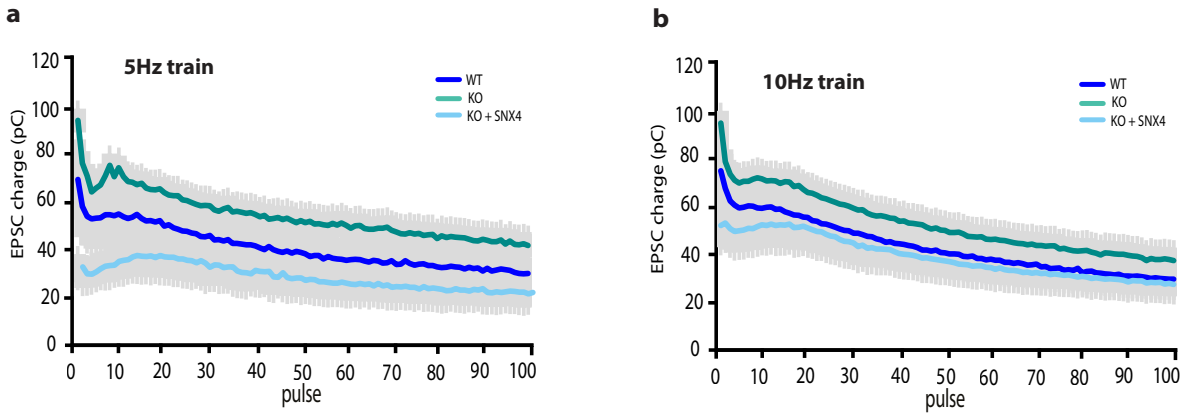

Supplementary figure 2: EPSC charge for 5 Hz and 10 Hz train stimulation.
(a) Mean EPSC charge trace for 100 AP at 5 Hz train. **(b)** Mean EPSC charge trace for 100 AP at 10 Hz train.

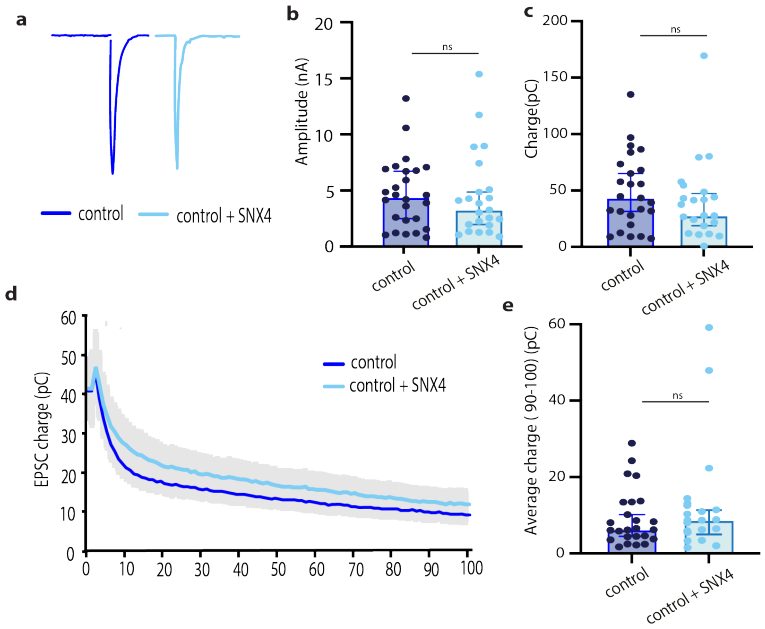

Supplementary 3: SNX4 overexpression does not affect first evoked EPSC or neurotransmission during sustained release. **(a)** Representative traces of the first evoked response for control and control+SNX4 upon stimulation. **(b)** Amplitude of first evoked response. **(c)** Charge of first evoked response. **(d)** Mean EPSC charge trace for 100 AP at 40 Hz train. **(e)** Average charge at pulse 90-100. Multilevel ANOVA with n = 22-26 neurons per group of N = 4-6 animals. Data points represent individual neurons; bar graph represents median + 95% confidence interval.

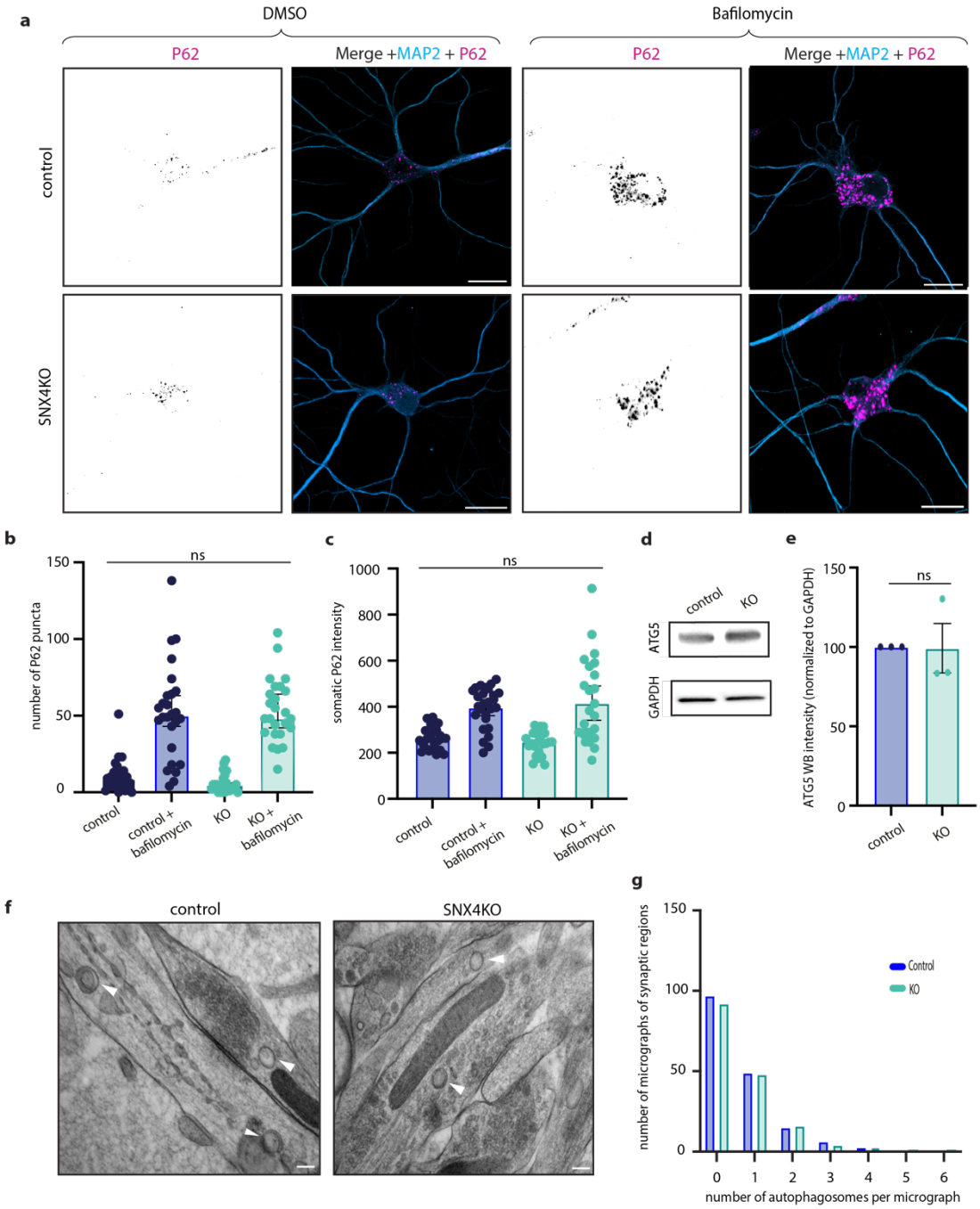

Supplementary 4: Autophagy markers remain unaffected upon SNX4 depletion.
(a) Typical example immunocytochemistry images of primary hippocampal neurons stained for P62 (magenta) and MAP2 (green) from control and SNX4 cKO mice with and without bafilomycin treatment. Scale bar = 20 µm. **(b)** P62 puncta control and KO. **(c)** P62 intensity measured in soma. **(d)** Western blot of ATG5 and actin for control and KO. **(e)** Quantification for total ATG5 expression levels normalized to GAPDH and control. **(f)** Typical example of autophagosomes characterized by double membrane in electron micrographs of control and KO. **(g)** Overview of number of micrographs of synaptic regions containing autophagosomes for control and KO. Bar graphs represent median with 95% CI. For (a,bc) n = 25-27 per group N=3, for (f-g) n = 165-170 photo's per group from N=3.

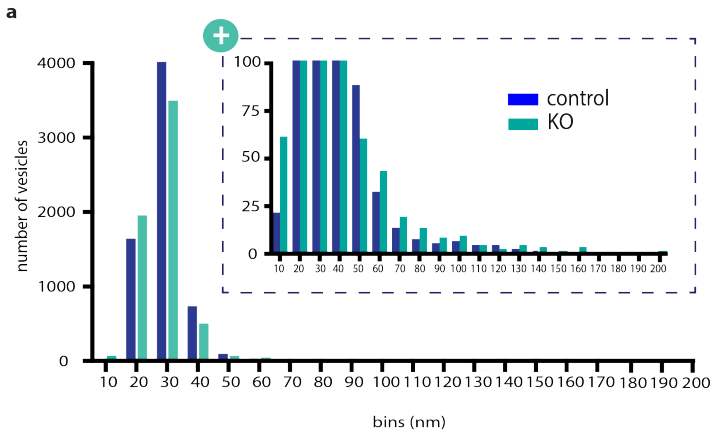

Supplementary 5: Histogram of vesicle size for control and SNX4KO synapses.
(a) Histogram of number of vesicles in bins per 10 nm.

Figure 1	n number (range neurons or synapses per group /animals)	mean	median	SEM	SD	significant test	p-value
snx4 wb	x/3	dcre = 100 21d cre = 9,913 18d cre = 16,87 14d cre = 32,52	dcre = 100 21d cre = 8,489 18d cre = 11,68 14d cre = 19,18	dcre = 0 21d cre = 4,943 18d cre = 9,817 14d cre = 25,52	dcre = 0 21d cre = 8,561 18d cre = 9,817 14d cre = 25,52	Ordinary one way anova	dcre-21d cre = 0,0003 dcre-18d cre = 0,0005 dcre-14d cre = 0,0019
snx4 fluorescence	38-42/6	control = 100,0 KO = 42,66	control = 98,74 KO = 37,46	control = 3,267 KO = 3,471	control = 21,17 KO = 21,40	mann-whitney test	p<0,0001
Dendrite length	32-36/6	control = 1530 KO = 1536	control = 1407 KO = 1389	control = 99,16 KO =109,6	control = 594,9 KO =620,2	mann-whitney test	p = 0,9077
# vamp2 puncta per neuron	35-41/6	control = 605,3 KO = 626,1	control = 536,0 KO =533,0	control = 40,23 KO =61,68	control = 257,6 KO = 364,9	mann-whitney test	p = 0,899
Figure 2							
Amplitude (pA)	25-34/4	control = 6081 KO = 7124 KO + SNX4 = 3508	control = 5272 KO = 6546 KO + SNX4 = 2908	control = 826,1 KO = 1076 KO + SNX4 = 439,6	control = 4817 KO = 5382 KO + SNX4 = 2198	multilevel anova + bonferroni correction	Con-KO = 1 Con-SNX4 = 0,061 KO-SNX4 = 0,0378
Charge (pC)	25-33/4	control = 88,53 KO = 121,7 KO + SNX4 = 57,38	control = 66,98 KO = 78,04 KO + SNX4 = 40,06	control = 15,61 KO = 21,34 KO + SNX4 = 9,295	control = 89,67 KO = 106,7 KO + SNX4 = 47,40	multilevel anova + bonferroni correction	Con-KO = 0,7718 Con-SNX4 = 0,4833 KO-SNX4 = 0,0584
Inter pulse Ratio pulse 25 (p2/p1)	25-33/4	control = 0,9813 KO = 0,8808 KO + SNX4 = 1,022	control = 0,9489 KO = 0,8515 KO + SNX4 = 1,017	control = 0,06983 KO = 0,04791 KO + SNX4 = 0,06540	control = 0,4012 KO = 0,2395 KO + SNX4 = 0,3582	multilevel anova	p = 0,2756
Inter pulse Ratio pulse 50 (p2/p1)	15-19/4	control = 1,088 KO = 0,9564 KO + SNX4 = 1,152	control = 0,9337 KO = 0,9157 KO + SNX4 = 1,138	control = 0,09870 KO = 0,05315 KO + SNX4 = 0,08174	control = 0,3823 KO = 0,2126 KO + SNX4 = 0,3563	multilevel anova	p = 0,198
Inter pulse Ratio pulse 100 (p2/p1)	32-38/4	control = 0,9123 KO = 0,8791 KO + SNX4 = 0,9327	control = 0,8729 KO = 0,8553 KO + SNX4 = 0,9168	control = 0,03475 KO = 0,03696 KO + SNX4 = 0,04336	control = 0,2142 KO = 0,2024 KO + SNX4 = 0,2453	multilevel anova	p = 0,9329
Inter pulse Ratio pulse 200 (p2/p1)	25-29/4	control = 0,8399 KO = 0,8045 KO + SNX4 = 0,8718	control = 0,8257 KO = 0,7830 KO + SNX4 = 0,8747	control = 0,03448 KO = 0,02499 KO + SNX4 = 0,03094	control = 0,1857 KO = 0,1369 KO + SNX4 = 0,1547	multilevel anova	p = 0,3914
Average charge (pulse 90-100) (p2/p1)	25-33/4	control = 8,562 KO = 18,15 KO + SNX4 = 9,098	control = 6,557 KO = 9,282 KO + SNX4 = 4,745	control = 1,115 KO = 3,665 KO + SNX4 = 1,545	control = 6,405 KO = 18,33 KO + SNX4 = 8,318	multilevel anova + bonferroni correction	Con-KO = 0,0045 Con-SNX4 = 1 KO-SNX4 = 0,0067
RRP estimate (pC)	25-34/4	control = 783,5 KO = 871,7 KO + SNX4 = 659,3	control = 453,3 KO = 486,1 KO + SNX4 = 581,0	control = 167,2 KO = 158,9 KO + SNX4 = 93,64	control = 975,1 KO = 794,7 KO + SNX4 = 512,9	multilevel anova	p = 0,2124
slope estimate (pC/s)	25-33/4	control = 8,953 KO = 18,67 KO + SNX4 = 9,513	control = 7,074 KO = 9,569 KO + SNX4 = 5,667	control = 1,155 KO = 3,755 KO + SNX4 = 1,589	control = 6,636 KO = 18,78 KO + SNX4 = 8,555	multilevel anova + bonferroni correction	Con-KO = 0,0051 Con-SNX4 = 1 KO-SNX4 = 0,0073
mEPSCs amplitude	16-27/4-6	control = -31,83 KO = -30,75 KO + SNX4 = -30,78	control = -30,61 KO = -31,64 KO + SNX4 = -31,60	control = 1,580 KO = 1,407 KO + SNX4 = 1,351	control = 8,208 KO = 5,627 KO + SNX4 = 5,404	multilevel anova	p =0,7411
mEPSCs frequency	16-27/4-6	control = 1,965 KO = 1,855 KO + SNX4 = 1,975	control = 1,769 KO = 1,509 KO + SNX4 = 1,290	control = 0,2647 KO = 0,3627 KO + SNX4 =0,5250	control = 1,349 KO = 1,451 KO + SNX4 = 2,100	multilevel anova	p = 0,8694
Figure 3							
Stim1 (F/F0)	21-24/3	control = 0,5590 KO = 0,5028	control = 0,5382 KO = 0,4864	control = 0,03406 KO = 0,01363	control = 0,1669 KO = 0,06247	multilevel anova	p = 0.1643
Stim2 (F/F0)	21-24/3	control = 0,5663 KO = 0,5097	control = 0,5404 KO = 0,4768	control = 0,05318 KO = 0,02385	control = 0,2605 KO = 0,1093	multilevel anova	p = 0.4062
NH4 intensity	21-24/3	control = 2,002 KO = 1,507	control = 1,887 KO = 1,473	control = 0,1539 KO = 0,1268	control = 0,7538 KO = 0,5810	multilevel anova	p = 0.0152
release fraction first stim	21-24/3	control = 0,1928 KO = 0,2262	control = 0,1937 KO = 0,2031	control = 0,008183 KO =0,01943	control = 0,04009 KO = 0,08906	multilevel anova	*p = 0.0954*
release fraction 2nd stim	21-24/3	control = 0,1858 KO = 0,2206	control = 0,1781 KO = 0,1850	control = 0,01210 KO = 0,01976	control = 0,05929 KO = 0,09056	multilevel anova	p = 0.1195
decay time tau first stim	21-24/3	control = 1,606 KO = 1,919	control = 1,691 KO = 1,807	control = 0,6841 KO = 0,1571	control = 3,351 KO = 0,7201	multilevel anova	p = 0.6617
decay time tau second stim	21-24/3	control = 2,472 KO = 1,584	control = 1,721 KO = 1,400	control = 0,9126 KO = 0,1740	control = 4,471 KO = 0,7972	multilevel anova	p = 0.3612
average active synapses	21-24/3	control = 60,88 KO = 45,97	control = 66,76 KO = 47,46	control = 5,375 KO = 4,562	control =26,33 KO = 20,91	multilevel anova	p = 0.3127
FM4-64 release	28-36/4	control = 18,27 KO = 16,57	control = 15,04 KO = 15,71	control = 1,719 KO = 1,625	control = 10,32 KO = 8,600	multilevel anova	p = 0.5103
FM4-64 uptake	28-36/4	control = 100,0 KO = 94,27	control = 99,98 KO = 96,50	control = 3,263 KO = 4,586	control = 19,58 KO = 24,27	multilevel anova	p = 0.2882
Figure 5							
vamp2 puncta per um	35-41/6	control = 0,4829 KO = 0,5289	control = 0,4196 KO = 0,4486	control = 0,02679 KO = 0,03598	control = 0,1715 KO = 0,2128	mann-whitney test	p = 0,5053
vamp2 intensity in neurites	35-41/6	control = 100,0 KO = 92,94	control = 97,53 KO = 86,62	control = 3,505 KO = 5,445	control = 22,44 KO = 33,12	Unpaired t test with Welch's correction	p = 0,28
Figure 6							
fraction docked	174-175/3	control = 4,974 KO = 6,353	control = 4,487 KO = 5,556	control = 0,2251 KO = 0,2992	control = 2,978 KO = 3,946	mann-whitney test	p = 0,0002
# docked normalized to AZ	174-175/3	control = 0,9119377 KO = 1,390216	control = 0,8270241 KO = 1,404846	control = 0,02914 KO = 0,03772	control = 0,3854 KO = 0,4976	mann-whitney test	p < 0,0001
# docked ccv	174-175/3	control = 6,269 KO = 8,190	control = 6 KO = 7	control = 0,3017 KO = 0,3380	control = 3,992 KO = 4,458	mann-whitney test	p < 0,0001
# total ccv	174-175/3	control = 157,2 KO = 160,5	control = 120 KO = 134,5	control = 8,425 KO = 7,726	control = 111,5 KO = 101,9	mann-whitney test	p = 0,3682
vesicle size 0-50	174-175/3	control = 29,34 KO = 28,48	control = 28,50 KO = 27,39	control = 0,1007 KO = 0,1277	control = 8,186 KO = 10,02	multilevel anova	p = <,0001
vesicle size 0-50 per synapse	174-175/3	control = 27,54 KO = 28,48	control = 28,67 KO = 28,02	control = 0,2044 KO = 0,2427	control = 2,727 KO = 3,238	mann-whitney test	p = 0,0007
vesicle size 50 plus per synapse	174-175/3	control = 72,38 KO = 75,89	control = 67,19 KO = 65,95	control = 3,075 KO = 2,991	control = 22,17 KO = 22,18	mann-whitney test	p = 0,3529
vesicle cluster area	174-175/3	control = 0,2193 KO = 0,1741	control = 0,1720 KO = 0,1510	control = 0,01283 KO = 0,008008	control = 0,1697 KO = 0,1056	mann-whitney test	p = 0,0322
actie zone length	174-175/3	control = 706,1 KO = 600,3	control = 617,3 KO = 538,7	control = 29,98 KO = 21,17	control = 396,6 KO = 279,2	mann-whitney test	p = 0,0248
PSD length	174-175/3	control = 701,9 KO = 589,5	control = 611,4 KO = 526,8	control = 30,10 KO = 20,95	control = 398,2 KO = 276,4	mann-whitney test	p = 0,0157
Supplementary 3							
first evoked ampltidue (pA)	23-26/3	control = 4629 SNX4 OE = 4629	control = 4347 SNX4 OE = 3217	control = 602,9 SNX4 OE = 775,5	control = 3074 SNX4 OE = 3719	multilevel anova + bonferroni correction	p = 0,81
first evoked charge (pC)	22-25/3	control = 48,73 SNX4 OE = 39,49	control = 43,36 SNX4 OE = 27,80	control = 6,558 SNX4 OE = 7,631	control = 32,79 SNX4 OE = 35,79	multilevel anova + bonferroni correction	p = 0,361
Average charge (pulse 90-100) (p2/p1)	21-25/3	control = 9,228 SNX4 OE = 12,17	control = 6,229 SNX4 OE = 8,734	control = 1,474 SNX4 OE = 3,193	control = 7,372 SNX4 OE = 14,63	multilevel anova	p = 0.787
Supplementary 4							
number of P62 puncta	25-27/3	control = 10,76 control +bafilomycin = 51,88 KO = 5,960 KO +bafilomycin = 53,24	control = 9,000 control +bafilomycin = 50,00 KO = 4,000 KO +bafilomycin = 48,00	control = 2,120 control +bafilomycin = 6,134 KO = 1,220 KO +bafilomycin = 4,137	control = 10,60 control +bafilomycin = 31,28 KO = 6,100 KO +bafilomycin = 20,68	Kruskall-Wallis Dunn's multilple comparison	p = >0.9999
somatic P62 intensity	25-27/3	control = 263,8 control +bafilomycin = 396,3 KO = 247,3 KO +bafilomycin = 415,6	control = 262,0 control +bafilomycin = 411,3 KO = 246,1 KO +bafilomycin = 360,8	control = 9,745 control +bafilomycin = 17,08 KO = 10,19 KO +bafilomycin = 36,19	control = 48,73 control +bafilomycin = 88,75 KO = 50,94 KO +bafilomycin = 181,0	Kruskall-Wallis Dunn's multilple comparison	p = >0.9999
ATG5 WB levels	3	control = 100,0 KO = 99,23	control = 100,0 KO = 83,89	control = 0 KO = 15,54	control = 0 KO = 26,92	Unpaired t test	p = 0,9628

867

868 **Supplementary table 1: Statistics overview**
869
870